Investigation of thermal features of two types of alkali-vapor cells pumped by a laser diode

Juhong Han (韩聚洪), You Wang (王 敝)*, He Cai (蔡 和), Wei Zhang (张 伟), Liangping Xue (薛亮平), and Hongyuan Wang (王宏元)

Southwest Institute of Technical Physics, Chengdu 610041, China

**Corresponding author: youwang_2007@aliyun.com*

Received March 25, 2014; accepted May 3, 2014; posted online September 11, 2014

We develop a new algorithm to evaluate the thermal features of a rubidium-vapor cell and a cesium-vapor cell pumped by the laser diode. The theoretical model is based on the principles of both heat transfer and laser kinetics. The obtained population density distribution and the radial temperature distribution are analyzed for both types of cells. It is thought that the theoretical results are logically reasonable and the mathematical precision is satisfactory in designing a real diode-pumped alkali laser (DPAL). The methodology is valuable in the construction of a high-powered DPAL in the future.

OCIS codes: 140.1340, 140.3430, 140.3460, 140.3480.

doi: 10.3788/COL201412.S20201.

The new concept of a diode-pumped alkali laser (DPAL) was first proposed by Krupke in 2001[1]. The DPAL active medium contains vapors of neutral alkali (normally used as potassium (K), rubidium (Rb), and cesium (Cs)) and several kinds of buffer gases. In a DPAL, an alkali atom along with the two electric-dipole-allowed transitions participates in the laser action and the typical three electronic level is formed as shown in Fig. 1. In the recent decade, numerous theoretical and experimental studies on a three-level lasing in DPALs have been performed by several research groups[2–10]. As the saturated number density of the alkali vapor is highly dependent on the cell temperature, the temperature distribution must greatly influence the homogeneity of a laser medium, that is, alkali vapor[11,12]. Therefore, investigating the thermal features of a laser diode (LD)-pumped cell is crucial for realization of a high-powered DPAL with high beam quality. So far, only two teams undertook research works in the field of studying thermal effects inside an alkali-vapor cell[13–17]. Pan calculated the temperature distribution by using a procedure with analyses of the heat transfer and the optical path difference under different pump powers. They utilized an assumed absorption coefficient to carry out the calculation and the lasing process was not taken into account in their model. It is thought that such a theoretical system might not be self-consistent in logic because the absorption coefficient is actually determined by the temperature distribution. Barmashenko and Rosenwaks examined the laser output characteristics by means of a kinetic evaluation. As the temperature is assumed as a constant in the lasing region, their algorithm might be too simple to obtain the accurate results. In this letter, we present the calculated results of two kinds of cells in a diode-pumped Rb-vapor laser (DPRVL) and a diode-pumped Ce-vapor laser (DPCVL) by using a synthetical model in which the principle of both heat transfer and laser kinetic are simultaneously involved.

We created a theoretical model by combining the procedure of heat transfer with that of laser kinetics to investigate the temperature distribution in the transverse section of two kinds of alkali-vapor cells. As shown in Fig. 2, a vapor cell is first separated to many coaxial cylinders to realize the accumulating calculation. A cyclic iterative approach is utilized to calculate the population densities. During the evaluation, some assumptions are made to simplify the calculation process: 1) The temperature of every cylinder keeps unchanged along the optical axis.

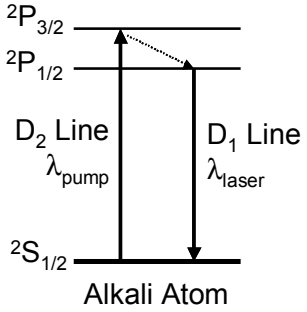

Fig. 1. Energy levers of an alkali atom for construction of a DPAL.

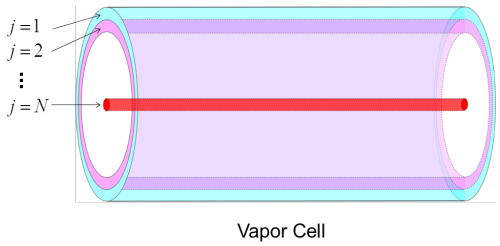

Fig. 2. Schematic illustration of the segmental process for an alkali-vapor cell.

2) The diameter of the alkali laser beam is a constant along the optical axis.
3) The radial pump distribution holds out a Gaussian intensity profile and keeps unchanged during the propagation inside the vapor cell.
4) The alkali metal is excessive inside the vapor cell to maintain a stable saturated vapor pressure.
5) Both end windows of a vapor cell bring no influences on the temperature results.

In Fig. 3, a flowchart of the whole algorithm is schematically illustrated. At first, we assume that the total heat transferred out from a vapor cell is P_{Thermal}. The generated heat and the population densities (n_1, n_2, and n_3) of every cylinder are calculated by means of a complex scheme in which both the procedure of laser kinetics and that of heat transfer are considered at the same time. If the given value of P_{Thermal} is equal to the total generated heat, $\sum_{\text{j=1}}^{N} Q_{\text{j}}$, in other words, if the following equation is tenable:

$$P_{\text{Thermal}} = \sum_{\text{j=1}}^{N} Q_{\text{j}}, \tag{1}$$

the temperature distribution and thermal features of an alkali-vapor cell can be obtained in the transverse section.

By using the theoretical model depictured in Fig. 3, we obtain the spatial distributions in population density and temperature of both a Rb cell and a Ce cell under the different conditions. The physical characteristics of an output laser beam are also analyzed for both types of DPALs by using the parameters listed in Table 1.

The distributions of population density of each energy level on the cross section are shown in Figs. 4(a)

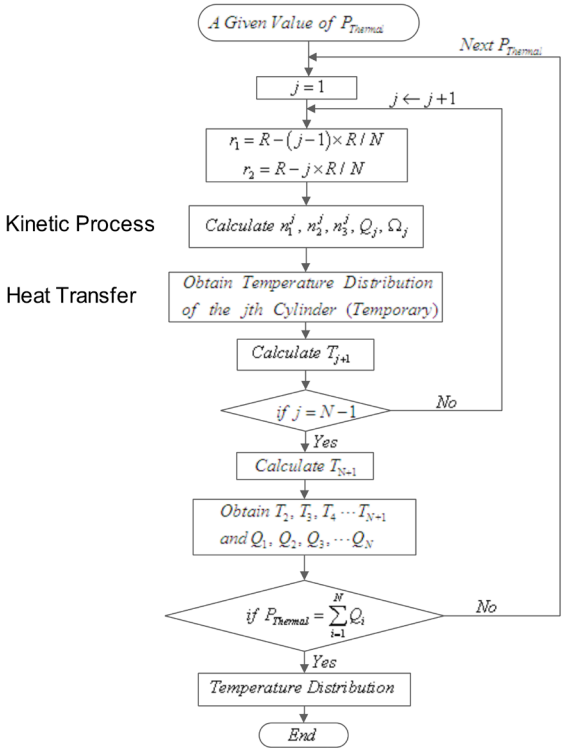

Fig. 3. Flowchart of the evaluation process.

Table 1. Parameters for Evaluating Physical Features of Two Kinds of DPALs

Parameter Description	**Values of a DPRVL**	**Values of a DPCVL**
Partial Pressure of Helium	478.8 Torr (0.63 atm)	478.8 Torr (0.63 atm)
Partial Pressure of Alkane	100 Torr (CH_4)	100 Torr (C_2H_6)
LD Linewidth at Full Width at Half Maximum (FWHM)	30 GHz	30 GHz
D_2 Transition Wavelength	780.25 nm	852.35 nm
D_1 Transition Wavelength	794.98 nm	894.59 nm
D_1 Radiative Lifetime	27.7 ns	34.9 ns
D_2 Radiative Lifetime	26.24 ns	30.5 ns
Pump Delivery Efficiency	0.9	0.9
Length of the Cell	25 mm	25 mm
Radius of the Cell	7.5 mm	7.5 mm
Temperature at the Cell Wall	383 K	383 K
Collisionally Broadened FWHM	14.4 GHz	9.03 GHz
Reflectance of the Output Coupler	0.3	0.3
One-way Transmission through Cavity	0.99	0.99

and (b) for the vapor cell in a DPRVL and Figs. 4(c) and (d) for that in a DPCVL, respectively. The waist radii of the pump beam are 75 and 300 μm while the pump power is 1 W, respectively.

In Fig. 4, n_0 represents the saturation concentration of the alkali vapor and its value exhibits an increasing tendency toward the cell center. By considering n_0 is highly dependent on the temperature distribution inside an enclosed cell, it can be easily deduced that the temperature around the cell center should be much higher than that at the cell surface.

In Fig. 4, we can find that abrupt variations occur in the population density curves and the inflexions are thought to locate at the lasing boundary of an alkali simulated irradiation beam. To maintain the population inversion, n_2 must be larger than n_1 in the lasing region. For a Ce cell, the bigger the spot size of a pump beam is, the lower is the n_3. The reason is that more electrons will be stimulated to the 6 $^2P_{3/2}$ level with high pump intensity. It will lead to the population accumulation in the 6 $^2P_{3/2}$ level as well as the relatively weak relaxation capability. One can see that an even higher pump intensity will not always bring about high laser emission for DPCVLs. As shown in Table 2, heat generated in a Ce cell does not monotonically increase with the pump intensity. However, for a Rb cell, the situation is somewhat different because the fine-structure mixing rate is sufficient enough to maintain a relatively fast relaxation process. Therefore, the population accumulation in the 5 $^2P_{3/2}$ level of a Rb atom is much

Table 2. Heat Generated in Two Types of Alkali Cells for Different Pump Beam Waists

Pump Beam Waist (μm)	Generated heat (W)	
	Rb Cell	Ce Cell
37.5	0.0146	0.0277
75	0.0141	0.0365
150	0.0127	0.0343
300	0.0098	0.0305

weaker than that in the 6 $^2P_{3/2}$ level of a Ce atom. It could be predicted that heat generated in a DPRVL monotonically increase with the pump intensity, which is different from the phenomenon of a DPCVL.

Next, we compare the population distributions in a Rb cell with those in a Ce cell for different pump powers. The distributions of population density of every energy level on the cross section are shown in Figs. 5(a) and (b) for the vapor cell in a DPRVL and Figs. 5(c) and (d) for that in a DPCVL, respectively. The pump powers are 20 and 50 W while the waist radius is 75 mm, respectively. It can be seen that the total number of population (saturation concentration) n_0 for 20 W are much lower than those for 50 W. It means that the population distribution will be strongly affected by the degree of strength of a pump beam. Additionally, under the same pump power, the saturation concentration for a Rb cell is much smaller than that for a Ce cell. The

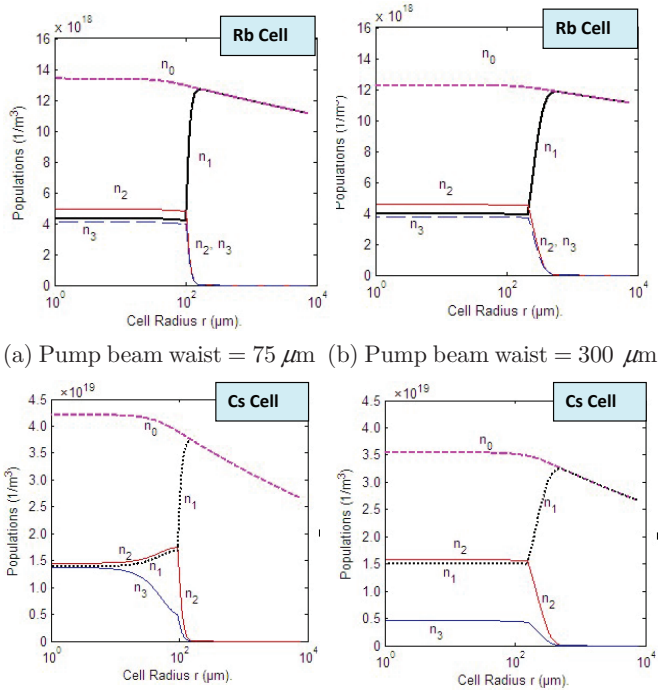

(a) Pump beam waist = 75 μm (b) Pump beam waist = 300 μm

(c) Pump beam waist = 75 μm (d) Pump beam waist = 300 μm

Fig. 4. Distributions of population density for a Rb cell and a Cs cell with the radii of the pump beams of 75 and 300 μm, respectively. The pump power is fixed to 1 W.

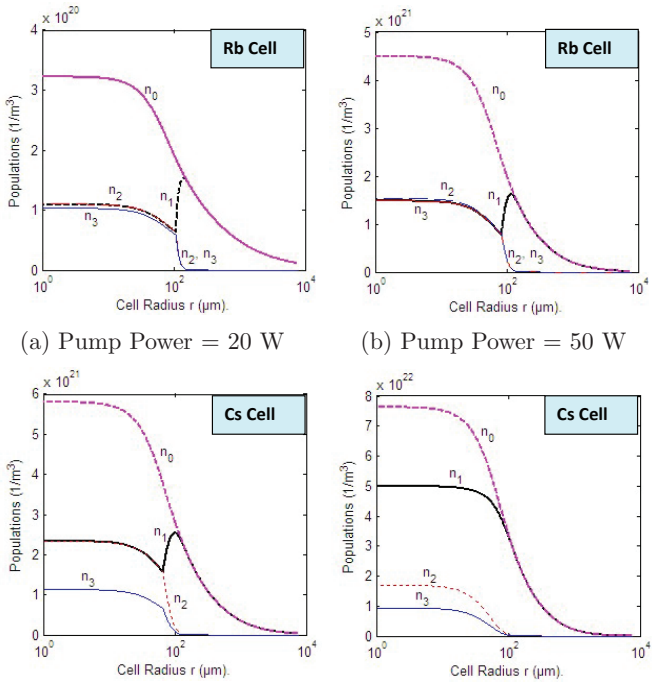

(a) Pump Power = 20 W (b) Pump Power = 50 W

(c) Pump Power = 20 W (d) Pump Power = 50 W

Fig. 5. Distributions of population densities for an Rb cell and a Cs cell with the pump powers of 20 and 50 W, respectively. The radius of the pump beam is fixed to 75 μm.

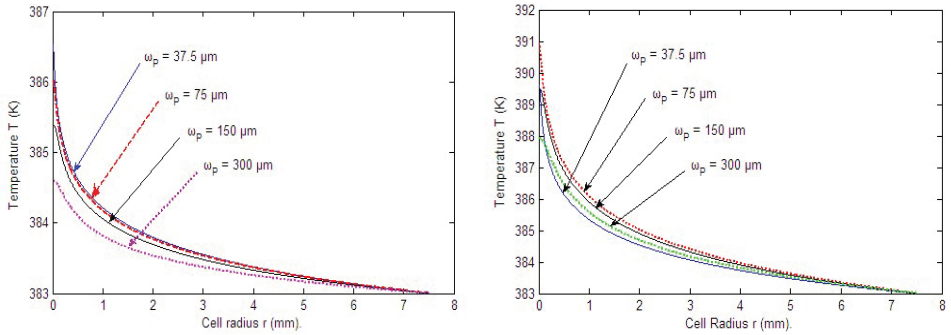

(a) a Rb cell (b) a Ce cell

Fig. 6. Temperature distributions for a Rb cell and a Ce cell. The pump power is fixed to 1 W.

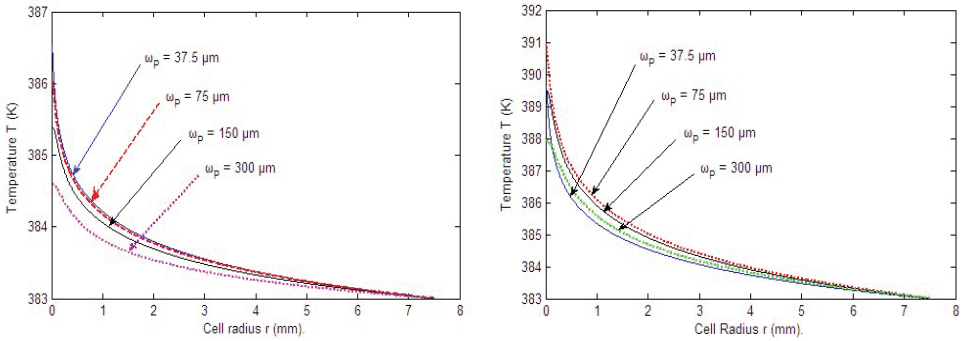

(a) a Rb cell (b) a Ce cell

Fig. 7. Temperature distributions for a Rb cell and a Ce cell. The pump beam waist is fixed to 75 μm.

laser irradiation of the Ce type even disappears when the pump power reaches to 50 W. This is because n_1 is too high to maintain the population inversion between $6^2P_{1/2}$ and $6^2S_{1/2}$ levels in a DPCVL.

We finally evaluate the temperature distributions at the cross section of a vapor cell as shown in Figs. 6 and 7. In Fig. 6, the waist radii of the pump beam are 37.5, 75, 150, and 300 μm with the pump power of 1 W, respectively. In Figs. 6(a) (for a Rb cell) and (b) (for a Cs cell), the distinct gradient can be observed in the temperature distributions. The maximum values appear on the central axis of both types of vapor cells.

As the relaxation rate from the 5 $^2P_{3/2}$ level to the 5 $^2P_{1/2}$ level in a Rb atom is high enough, the temperature gradient obviously increases with the pump intensity. But for a Ce atom, small-pump intensity will not always result in more heat generation. In Fig. 7, the pump powers are 1, 10, 20, and 50 W with the pump waist radius of 75 μm, respectively. It can be seen that the temperature gradient increases obviously with the pump power for two types of cells. The temperature gradient of a Rb cell (Fig. 7(a)) is somewhat gentler than that of a Ce cell (Fig. 7(b)). This should be caused by the fact that heat generated in a Rb cell is much less than that of a Cs cell (Table 3).

Figure 8 denotes the relationship between the pump power and the output power as well as the optical–optical conversion efficiency for a DPRVL and a DPCVL, respectively. In fig. 8, it is easy to find that an even higher pump power might arouse decrease in the laser output. The laser emission even vanishes when the pump power is higher than 220 W for a DPRVL and 40 W for a DPCVL, respectively.

The optimum values of the pump power for achieving the highest laser output and the highest optical–optical conversion efficiency are different. As generated heat is mainly caused by the gap between the $n^2P_{3/2}$ and $n^2P_{1/2}$ levels, the optical–optical conversion efficiency for a DPRVL is higher than that for a DPCVL because of the relatively light thermal effect.

Table 3. Heat Generated in Two Kinds of Alkali Cells with Different Pump Powers

Pump Power (W)	**Generated Heat (W)**	
	Rb	**Cs**
1	0.0141	0.0365
10	0.1615	0.3547
20	0.3174	1.2125
50	0.6885	—
100	1.0344	—
200	1.4340	—

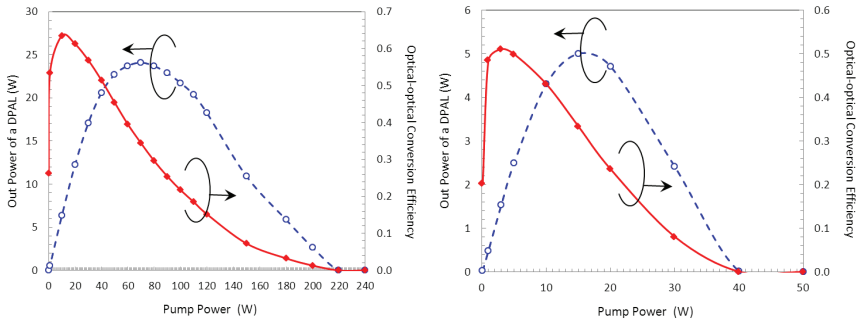

(a) a Rb cell (b) a Ce cell

Fig. 8. Pump power versus output power and optical–optical conversion efficiency for a DPRVL and a DPCVL. The pump beam waist is fixed to 75 μm.

In conclusion, we present the results of theoretical analyses on the thermal features of two kinds of alkali cells pumped by a LD. A theoretical model is developed by combining the procedure of laser kinetics and that of heat transfer together. The calculation results for a Rb cell are compared with those for a Ce cell in population and temperature distributions in the cross section. It can be seen that heat generated in a Rb cell is less than that generated in a Ce cell, since the gap between two upper energy levels of a Rb atom is less than a half of that of a Cs atom. The output characteristics of two types of DPAL systems are also investigated in detail. The results reveal that the difference in physical features between Rb and Cs atoms is a key point to regulate the performances of two kinds of DPALs. We present a relatively appropriate explanation on the thermal features of a DPAL and another model is being set up for the transverse pump configuration, which we are going to present in the future.

References

1. W. F. Krupke, U.S. Patent No. 6, **643,** 311.
2. W. F. Krupke, R. J. Beach, V. K. Kanz, and S. A. Payne, Opt. Lett. **28,** 2336 (2003).
3. R. J. Beach, W. F. Krupke, V. K. Kanz, and S. A. Payne, J. Opt. Soc. Am. B. **21,** 2151 (2004).
4. R. H. Page, R. J. Beach, and V. K. Kanz, Opt. Lett. **31,** 353 (2006).
5. Y. Wang, T. Kasamatsu, Y. Zheng, H. Miyajima, H. Fukuoka, S. Matsuoka, M. Niigaki, H. Kubomura, T. Hiruma, and H. Kan, Appl. Phys. Lett. **88,** 141112 (2006).
6. B. V. Zhdanov and R. J. Knize, Opt. Lett. **32,** 2167 (2007).
7. Y. Wang, M. Niigaki, H. Fukuoka, Y. Zheng, H. Miyajima, S. Matsuoka, H. Kubomura, T. Hiruma, and H. Kan, Phys. Lett. A. **360,** 659 (2007).
8. Z. Yang, H. Wang, Q. Lu, W. Hua, and X. Xu, Opt. Express **19,** 23118 (2011).
9. A. V. Bogachev, S. G. Garanin, A. M. Dudov, V. A. Yeroshenko, S. M. Kulikov, G. T. Mikaelian, V. A. Panarin, V. O. Pautov, A. V. Rus, and S. A. Sukharev, Quantum Electron. **42,** 95 (2012).
10. C. A. Rice, G. E. Lott, and G. P. Perram, Appl. Opt. **51,** 8102 (2012).
11. D. A. Steck, "Rubidium 85 D line data," http://steck.us/alkalidata
12. D. A. Steck, "Cesium D line data," http://steck.us/alkalidata
13. Q. Zhu, B. L. Pan, L. Chen, Y. J. Wang, and X. Y. Zhang, Opt. Commun. **283,** 2406 (2010).
14. Y. F. Liu, B. L. Pan, J. Yang, Y. J. Wang, M. H. Li, IEEE J. Quantum Electron. **48,** 485 (2012).
15. B. D. Barmashenko and S. Rosenwaks, Opt. Lett. **37,** 3615 (2012).
16. B. D. Barmashenko and S. Rosenwaks, Appl. Phys. Lett. **102,** 141108 (2013).
17. B. D. Barmashenko and S. Rosenwaks, J. Opt. Soc. Am. B **30,** 1118 (2013).